J. Fluid Mech. (1993), *vol.* 251, *pp.* 203–218

A wake singularity potential flow model for airfoils experiencing trailing-edge stall

By W. W. H. YEUNG[1] AND G. V. PARKINSON[2]

[1] Nanyang Technological University, Singapore

[2] Department of Mechanical Engineering, University of British Columbia, Vancouver, Canada V6T 1Z4

(Received 28 April 1992 and in revised form 1 December 1992)

An incompressible inviscid flow theory for single and two-element airfoils experiencing trailing-edge stall is presented. For the single airfoil the model requires a simple sequence of conformal transformations to map a Joukowsky airfoil, partially truncated on the upper surface, onto a circle over which the flow problem is solved. Source and doublet singularities are used to create free streamlines simulating shear layers bounding the near wake. The model's simplicity permits extension of the method to airfoil-flap configurations in which trailing-edge stall is assumed on the flap. Williams' analytical method to calculate the potential flow about two lifting bodies is incorporated in the Joukowsky-arc wake-singularity model to allow for flow separation. The theoretical pressure distributions from these models show good agreement with wind-tunnel measurements.

1. Introduction

Although computational fluid dynamics (CFD) has become a standard tool for solving complex physical problems in theoretical aerodynamics, there are still important roles for classical analytical methods, for example in providing comparison models (Bearman, Graham & Kalkanis 1989) and exploring different boundary conditions (Parkinson & Yeung 1987, hereinafter referred to as P&Y). Two-dimensional incompressible potential flow continues to be a useful branch of fluid mechanics for the study of the aerodynamics of airfoils at low speed, even for problems of separated flow such as airfoils near stall. In such problems it is realistic to assume that the portion of the airfoil surface exposed to the separated wake is at the constant separation pressure, and the shear layers bounding the wake can be simulated by free streamlines. One can then solve for the airfoil pressure loading and the flow pattern outside the wake. In this process analytical methods can be very effective through the use of the powerful properties of singularities in creating flow models and conformal mapping in solving the resulting boundary value problems.

The present paper deals with two new applications to airfoil aerodynamics of an analytical method of this type originally developed for symmetrical bluff-body flows proposed by Parkinson & Jandali (1970), and recently extended to flows past airfoils with spoilers or split flaps (P&Y). In the latter, the criterion of finite curvature (or pressure gradient) of the boundary streamline at separation is shown to be successful in eliminating the empirical specification of the separation point and provides a reasonable pressure distribution for the case of turbulent separation on a circular cylinder, compared with experimental data from Nakamura & Tomonari (1982).

Although less satisfactory results are obtained when the criterion is applied to airfoils with lower-surface split flaps, more encouraging findings are obtained by incorporating a similar idea into the design of low-speed airfoils, as reported by Ormsbee & Maughmer (1986). As a result, this criterion is further tested in these two new applications. Both applications of the method are to the problem of airfoil trailing-edge stall.

Trailing-edge stall, studied by McCullough & Gault (1951), occurs for some airfoil profiles and is associated with turbulent separation moving progressively forward from the trailing edge with increasing angle of attack. The chordwise pressure distribution is characterized by a high suction peak near the leading edge of the airfoil followed by a region of nearly constant pressure, indicative of flow separation, in the portion near the trailing edge. Previously, Schmieden (1940) proposed a hodograph method to model flow past a flat-plate airfoil exhibiting this type of stall, requiring tangential separation from the suction side as well as from the trailing edge to form an infinite wake. Subsequently, numerical methods for airfoil stall utilizing surface singularities were pioneered by Jacob (1969, 1987). This paper describes an analytical model of a different kind. The ultimate use of the model would be in an iterative calculation with a boundary-layer method to produce a prediction of the airfoil loading without empiricism.

2. Two models for trailing-edge stall

The Joukowsky airfoil profile used in P & Y (camber = 2.4%; thickness = 11% of chord) experiences trailing-edge stall and is used here as the prototype airfoil for a wake singularity model of the partially developed stall. The objective, given the separation point and the surface wake pressure coefficient C_{p_b} assumed constant, is to predict the resulting airfoil pressure distribution and the shape of the separating streamlines. In fact, two wake-singularity models have been developed to simulate the partially stalled flow, using two different mapping sequences and two flow models. The first, or vanishing spoiler, model is essentially a modification of the spoiler model in P & Y. Here the spoiler length is made very small and its angle δ is set at zero so that the spoiler tip represents the point of tangential separation of the partially stalled flow. This requires a modified sequence of conformal transformations from that in P & Y, but uses the same flow model in the final circle plane. It leads to a good prediction of airfoil pressure distribution, but an unsatisfactory prediction of separation streamline shape, so the model is not presented in detail here (see Yeung 1990).

The second, or Joukowsky arc, model was devised to exploit a simpler mapping sequence. It avoids the artificiality of a small zero-inclination spoiler simulating the separation region, and gives a better initial shape to the separating streamline.

2.1. *Joukowsky arc*

The mapping sequence is shown in figure 1. Using the fact that the portion of the body exposed to the wake is ignored in the flow model, part of it is truncated to create tangential separation at point A. The contour in the Z_1-plane is a circular-arc slit, centred in the second quadrant. A standard Joukowsky transformation maps it into a Joukowsky airfoil profile slit omitting the upper surface between points A and B. A is the upper-surface separation point in the stall problem and B is the upstream end of a trailing-edge portion of the upper surface lying in the wake region of the flow, and required by the mapping method as explained below. A translation and rotation to the Z_2-plane then recreates the circular-arc slit of the original wake source model for the

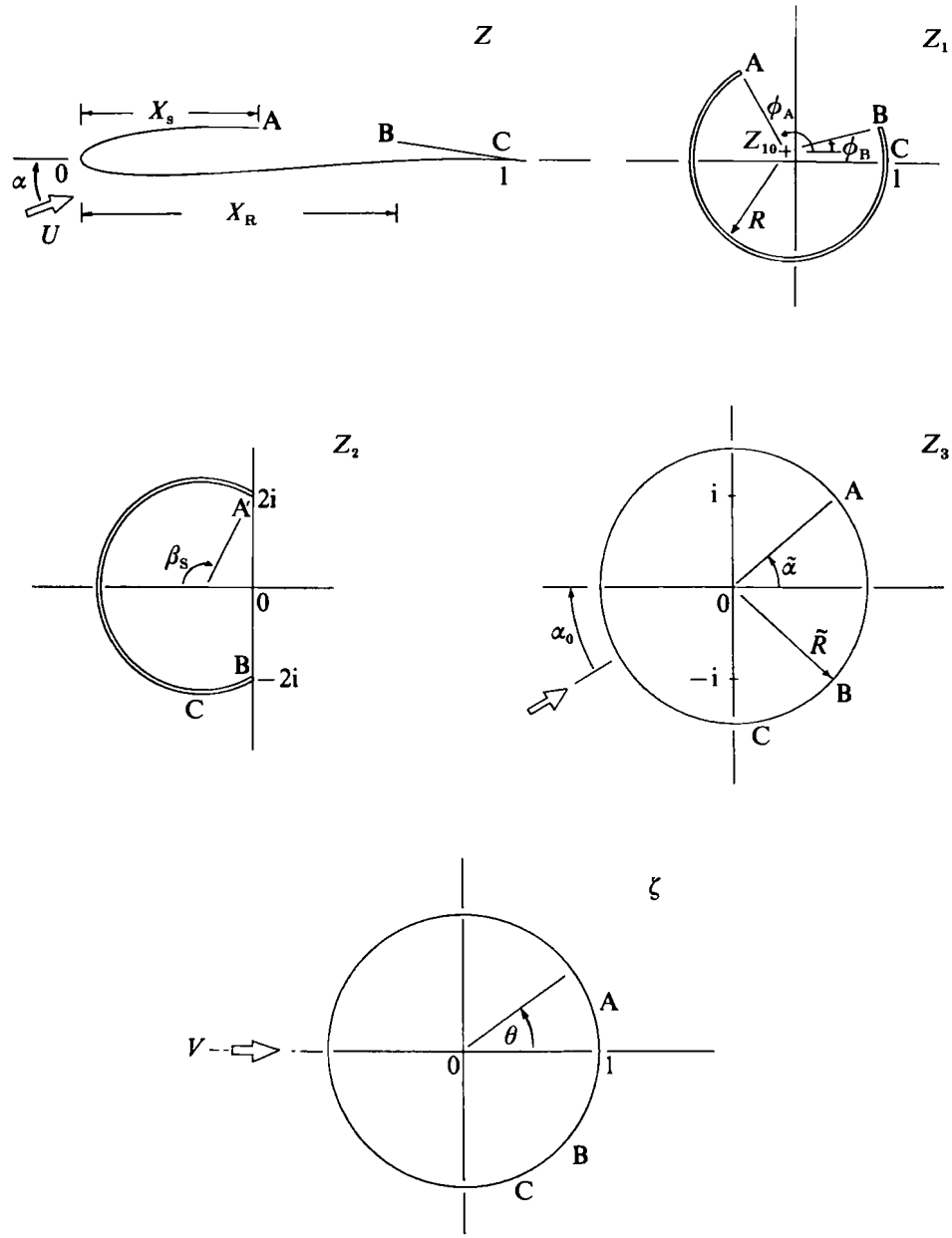

FIGURE 1. Mapping sequence for Joukowsky-arc model of airfoil experiencing trailing-edge stall.

circular cylinder flow in Parkinson & Jandali, and a second Joukowsky transformation maps the slit into a circle. Finally, this is rotated to the ζ-plane (so that the approach velocity is in the direction of the real axis), where the flow problem is solved. The transformation equations are

$$Z = A_1(Z_1 + 1/Z_1) + B_1, \tag{2.1}$$

$$Z_1 = C_1 Z_2 + D_1, \tag{2.2}$$

$$Z_2 = Z_3 - \cot\tilde{\alpha} - 1/(Z_3 - \cot\tilde{\alpha}), \tag{2.3}$$

$$Z_3 = \tilde{R} e^{i\alpha_0} \zeta, \tag{2.4}$$

where

$$A_1 = \frac{1}{2+\tilde{L}_1}, \quad B_1 = \frac{\tilde{L}_1}{2+\tilde{L}_1}, \quad \tilde{L}_1 = 2\epsilon + \frac{1}{1+2\epsilon},$$

$$C_1 = \frac{R}{2}\exp\left[\mathrm{i}\left(\frac{\phi_A+\phi_B}{2}\right)\right]\sin\left(\frac{\phi_A-\phi_B}{2}\right), \quad D_1 = R\exp\left[\mathrm{i}\left(\frac{\phi_A+\phi_B}{2}\right)\cos\left(\frac{\phi_A-\phi_B}{2}\right)+Z_{10}\right.,$$

$$\beta_S = \pi - \frac{\phi_A-\phi_B}{2}, \quad \tilde{\alpha} = \frac{\pi-\beta_S}{2}, \quad \tilde{R} = \operatorname{cosec}\tilde{\alpha}$$

$$R = |1-Z_{10}|, \quad Z_{10} = (-\epsilon, \mu).$$

Although the flow near and the pressure distribution along the arc BC predicted by the model are not of interest since the arc lies in the wake region, it was necessary to create the arc in the mapping to separate points B and C, which are critical points of different mappings in the sequence. The length X_R in figure 1 is an adjustable parameter.

Two additional mappings are required for an arbitrary airfoil profile. A Joukowsky transformation would map the wetted surface of the profile and the trailing-edge portion of the upper surface into a near circular arc. Then a true circular arc like that in the Z_1-plane can be generated by the series transformations of Theodorsen (1931) or James (see Halsey 1982). A finite trailing-edge angle of the profile can be made a cusp by modifying the portion on the upper surface, which is exposed to the wake and does not affect the present model.

2.2. *Flow model and results*

The flow model in the ζ-plane is similar to the 2-source model in P & Y, but one of the sources is replaced by a doublet tangent to the circle, which was found to be more effective. The complex velocity in the ζ-plane is

$$W(\zeta) = V\left\{\left(1-\frac{1}{\zeta^2}\right)+\mathrm{i}\frac{\gamma}{\zeta}+\frac{q_D\,\mathrm{i}\,\mathrm{e}^{\mathrm{i}\delta_D}}{(\zeta-\mathrm{e}^{\mathrm{i}\delta_D})^2}+q_S\left[\frac{1}{\zeta-\mathrm{e}^{\mathrm{i}\delta_S}}-\frac{1}{2\zeta}\right]\right\}, \tag{2.5}$$

where q_D and δ_D are respectively the strength and angular location (on $|\zeta| = 1$) of the doublet, δ_S is the location of the remaining double source on the circle, q_S is the strength of the double source and its image sink, and γ is the strength of the vortex (for circulation). The pressure coefficient C_p in the Z-plane is defined as

$$C_p = \frac{p-p_\infty}{\frac{1}{2}\rho U^2}, \tag{2.6}$$

where p and p_∞ are the local and upstream undisturbed pressures and $\frac{1}{2}\rho U^2$ is the dynamic pressure. Through Bernoulli's equation, C_p can then be written as

$$C_p = 1-\left|\frac{W(Z)}{U}\right|^2 = 1-\left(\frac{|W(\zeta)|}{U|\mathrm{d}Z/\mathrm{d}\zeta|}\right)^2. \tag{2.7}$$

The boundary conditions used to solve for q_D, q_S, γ, δ_D, δ_S are: (i) $W(\zeta) = 0$ at $\zeta = \mathrm{e}^{\mathrm{i}\theta_C}$ and $\zeta = \mathrm{e}^{\mathrm{i}\theta_A}$, where θ_C and θ_A are angular locations of C and A defined in figure 1; (ii) $C_p = C_{p_b}$ at these two locations in the Z-plane, where C_{p_b} is the pressure in the wake, given empirically, and (iii) finite C_p gradient at separation; that is, from P & Y,

$$f_1''f_2'-f_2''f_1' = 0 \tag{2.8}$$

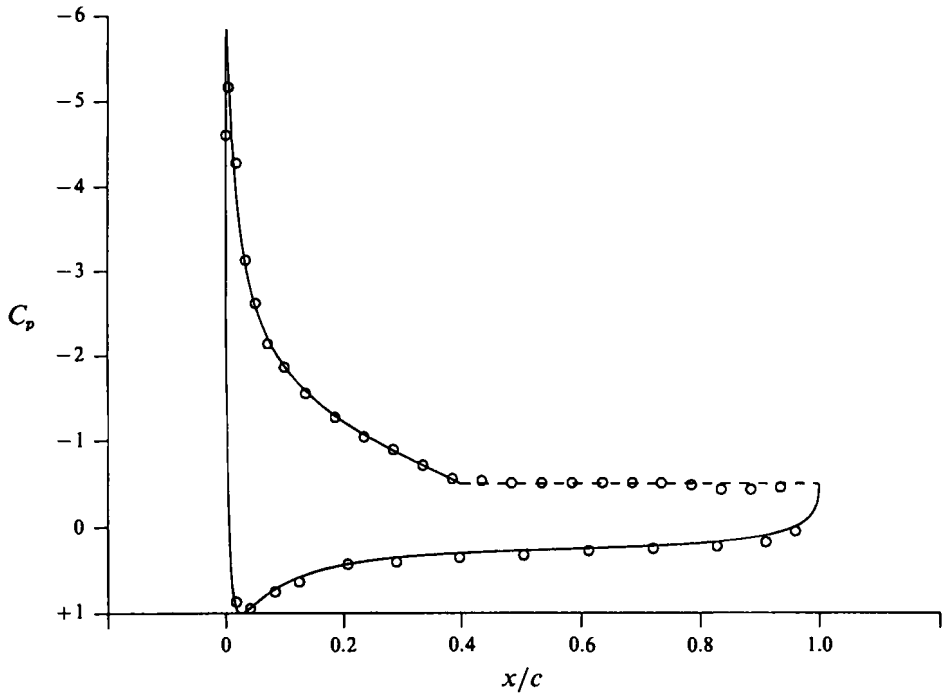

FIGURE 2. Pressure distribution for Joukowsky airfoil with trailing-edge stall, $\alpha = 14°$. —— theory, $X_S = 0.40$, C_p (wake) $= -0.50$, $X_R = 0.95$; ○, experiment.

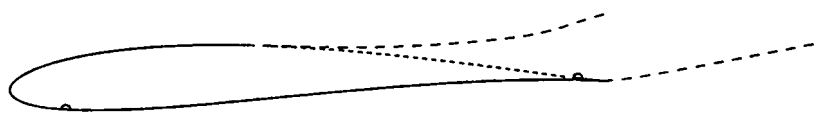

FIGURE 3. Separation streamlines in Joukowsky-arc model, $\alpha = 14°$, for the example of figure 2.

at $\zeta = e^{i\theta_A}$ where $f_1 = |W(\zeta)|$ and $f_2 = |dZ/d\zeta|$, and the derivative is taken with respect to θ.

Because both $W(\zeta)$ and $dZ/d\zeta$ vanish at the critical points, their pressure coefficients have to be evaluated by using l'Hôpital's rule,

$$C_p|_{C,A} = 1 - \left| \frac{(d/d\zeta)\, W(\zeta)}{U(d/d\zeta)(dZ/d\zeta)} \right|^2. \tag{2.9}$$

Figure 2 compares the calculated C_p distribution, using $X_R = 0.95$, with experimental data. The experiments were conducted using the same Joukowsky airfoil model, wind tunnel, and test conditions as described in P & Y. The Reynolds number was 5×10^5. The agreement is good. The separation streamline is shown in figure 3. The two symbols in the diagram represent the locations of the doublet and the source on the slit. Varying the value of X_R has the effect of changing the overall lift and the shape of the streamlines. For $X_R = 0.99$, the corresponding C_p distribution and the streamlines are still acceptable, as shown in figures 4 and 5. However, $X_R = 1$ (segment BC eliminated) must be avoided, and too low a value of X_R produces a separation streamline shape unlike that of the actual separating shear layer, so it is recommended to choose $0.85 < X_R < 1$.

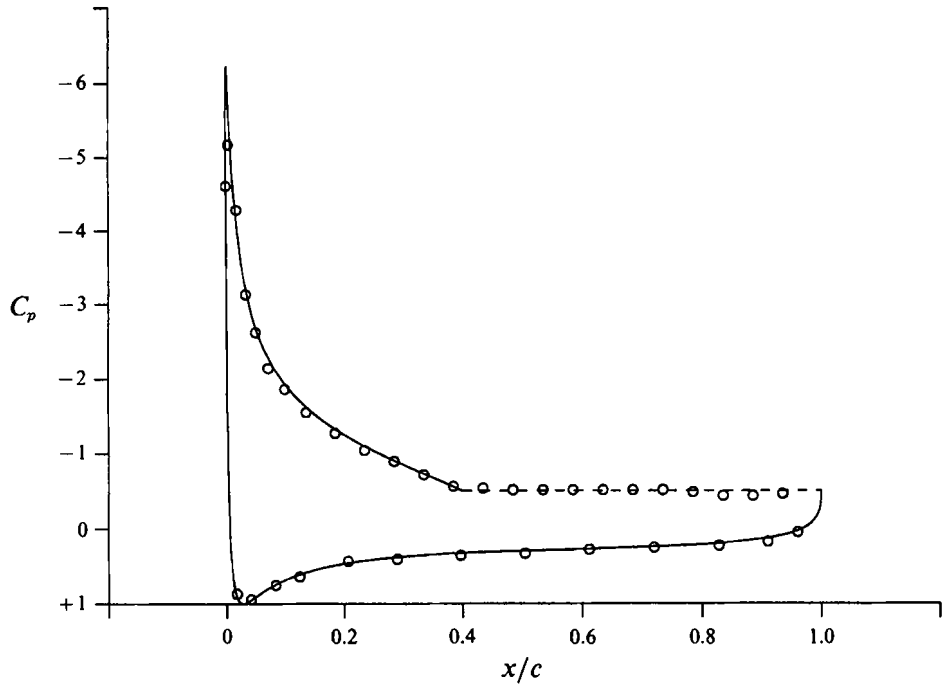

FIGURE 4. Pressure distribution for Joukowsky airfoil with trailing-edge stall, $\alpha = 14°$. —— theory, $X_S = 0.40$, C_p (wake) $= -0.50$. $X_R = 0.99$; ○, experiment.

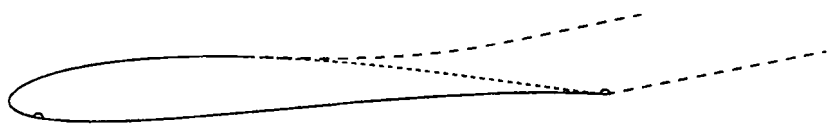

FIGURE 5. Separation streamlines in Joukowsky-arc model, $\alpha = 14°$, for the example of figure 4.

3. Two-element airfoils near stall

3.1. *Calculations for two lifting circles by Williams' exact method*

As pointed out by Williams (1971), the method of calculating the potential flow about multiply-connected regions can be very complex, involving the use of elliptic functions. Hence, he has devised a method to systematically establish the potential flow about two lifting circles by the method of images based on Milne–Thomson's circle theorem. The overall flow is then represented simply by a sequence of three components: a streaming flow past both circles, a flow with unit circulation around the first circle, and one around the second circle. Each component is represented by an infinite series which converges absolutely. Then, the two circles are mapped conformally into two airfoils by Karman–Trefftz transformations with the circulation on each element determined by the Kutta condition at the trailing edge.

The complex potential for the streaming flow of velocity V approaching two circles at an angle of attack δ_0 can be written as

$$F^S(\zeta) = V\left[h(\zeta) + \sum_{j=0}^{\infty} \{g_j(\zeta) + f_j(\zeta)\}\right], \tag{3.1}$$

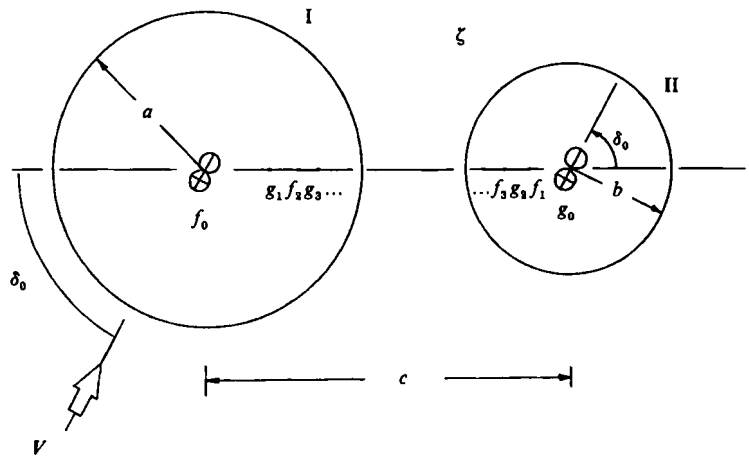

FIGURE 6. Geometry of two circles in streaming flow with doublet images.

where $$h(\zeta) = \zeta e^{-i\delta_0},$$

$$f_0(\zeta) = \frac{K_0}{\zeta - D_0}, \quad K_0 = a^2 e^{i\delta_0}, \quad D_0 = 0,$$

$$g_0(\zeta) = \frac{J_0}{\zeta - L_0}, \quad J_0 = b^2 e^{i\delta_0}, \quad L_0 = c.$$

In general, $$g_j(\zeta) = \frac{J_j}{\zeta - L_j}, \quad f_j(\zeta) = \frac{K_j}{\zeta - D_j},$$

where for $j = 1, 3, 5, \ldots$

$$J_j = -\frac{\bar{J}_{j-1} a^2}{L_{j-1}^2}, \quad L_j = \frac{a^2}{L_{j-1}}, \quad K_j = -\frac{\bar{K}_{j-1} b^2}{(c - D_{j-1})^2}, \quad D_j = c - \frac{b^2}{c - D_{j-1}},$$

and for $j = 2, 4, 6, \ldots$

$$J_j = -\frac{\bar{J}_{j-1} b^2}{(c - L_{j-1})^2}, \quad L_j = c - \frac{b^2}{c - L_{j-1}}, \quad K_j = -\frac{\bar{K}_{j-1} a^2}{D_{j-1}^2}, \quad D_j = \frac{a^2}{D_{j-1}}$$

and the overbar denotes the complex conjugate.

Figure 6 depicts the sequence of image doublets for the two circles.

If $p_j(\zeta)$ and $q_j(\zeta)$ respectively denote the image systems of a vortex flow of unit strength around circles I and II in figure 7, then the complex potentials for the flow around individual circles are

$$F^{c_1}(\zeta) = \sum_{j=0}^{\infty} p_j(\zeta), \quad F^{c_2}(\zeta) = \sum_{j=0}^{\infty} q_j(\zeta). \tag{3.2}$$

For $p_j(\zeta)$,

$$p_0(\zeta) = \frac{i}{2\pi} \ln \zeta, \quad p_1(\zeta) = \frac{i}{2\pi} \ln (\zeta - L_1), \quad p_2(\zeta) = -\frac{i}{2\pi} \ln (\zeta - L_2),$$

$$L_1 = c, \quad L_2 = c - b^2/c,$$

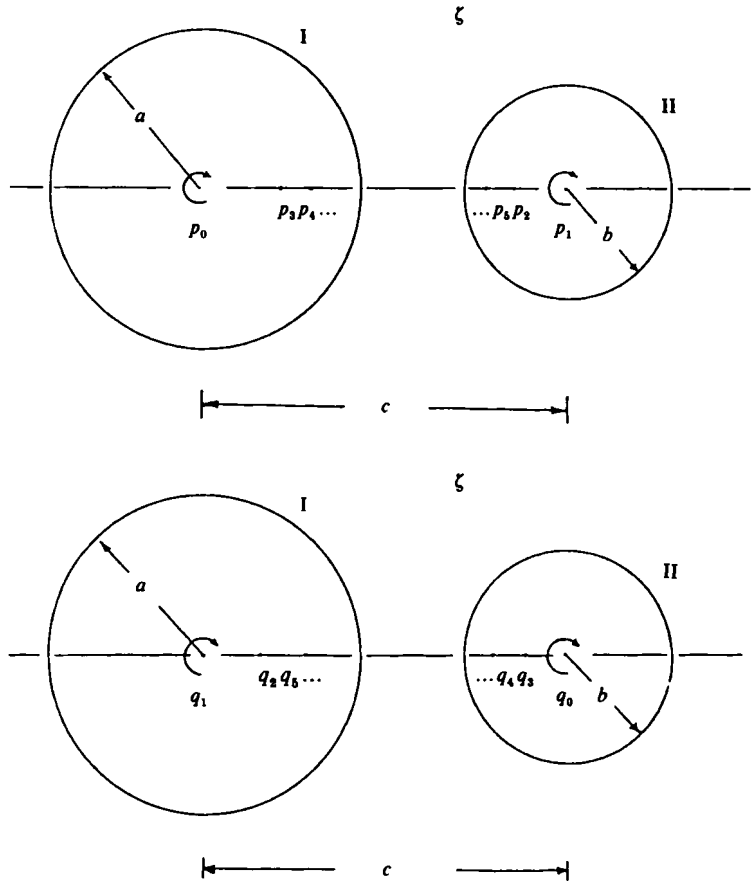

FIGURE 7. Geometry of two circles with vortex images.

and for $j = 3, 7, 11, \ldots,$

$$p_j(\zeta) = -\frac{\mathrm{i}}{2\pi}\ln(\zeta - L_j), \quad p_{j+1}(\zeta) = \frac{\mathrm{i}}{2\pi}\ln(\zeta - L_{j+1}),$$

$$L_j = \frac{a^2}{L_{j-2}}, \quad L_{j+1} = \frac{a^2}{L_{j-1}},$$

while for $j = 5, 9, 13, \ldots,$

$$p_j(\zeta) = \frac{\mathrm{i}}{2\pi}\ln(\zeta - L_j), \quad p_{j+1}(\zeta) = -\frac{\mathrm{i}}{2\pi}\ln(\zeta - L_{j+1}),$$

$$L_j = c - \frac{b^2}{c - L_{j-2}}, \quad L_{j+1} = c - \frac{b^2}{c - L_{j-1}}.$$

For $q_j(\zeta)$,

$$q_0(\zeta) = \frac{\mathrm{i}}{2\pi}\ln(\zeta - d_0), \quad q_1(\zeta) = \frac{\mathrm{i}}{2\pi}\ln(\zeta - d_1), \quad q_2(\zeta) = -\frac{\mathrm{i}}{2\pi}\ln(\zeta - d_2),$$

where $$d_0 = c, \quad d_1 = 0, \quad d_2 = a^2/c,$$

and for $j = 3, 7, 11, \ldots$,

$$q_j(\zeta) = -\frac{\mathrm{i}}{2\pi}\ln(\zeta - d_j), \quad q_{j+1}(\zeta) = \frac{\mathrm{i}}{2\pi}\ln(\zeta - d_{j+1}),$$

where

$$d_j = c - \frac{b^2}{c - d_{j-2}}, \quad d_{j+1} = c - \frac{b^2}{c - d_{j-1}},$$

for $j = 5, 9, 13, \ldots$,

$$q_j(\zeta) = \frac{\mathrm{i}}{2\pi}\ln(\zeta - d_j), \quad q_{j+1}(\zeta) = -\frac{\mathrm{i}}{2\pi}\ln(\zeta - d_{j+1}),$$

where

$$d_j = \frac{a^2}{d_{j-2}}, \quad d_{j+1} = \frac{a^2}{d_{j-1}}.$$

The total complex potential is obtained by superposition,

$$F(\zeta) = F^{\mathrm{S}}(\zeta) + \gamma_1 V F^{\mathrm{c}_1}(\zeta) + \gamma_2 V F^{\mathrm{c}_2}(\zeta), \tag{3.3}$$

where $\gamma_1 V$ and $\gamma_2 V$ are the vortex strengths around the first and second circles respectively. The horizontal (u) and vertical (v) velocity components in the ζ-plane containing the circles are given by

$$u - \mathrm{i}v = \frac{\mathrm{d}}{\mathrm{d}\zeta} F(\zeta) \tag{3.4}$$

from which the normal velocity (U_r) and tangential velocity (U_θ) components at a point on the surface of a circle are

$$U_r = u\cos\theta + v\sin\theta, \tag{3.5}$$

$$U_\theta = v\cos\theta - u\sin\theta, \tag{3.6}$$

where θ denotes the angular coordinate of this particular circle with respect to its own centre.

If sufficient terms are included in the series of $F(\zeta)$, then the normal velocity on the surface of each circle should be close to zero. In the present work, the series is truncated once the accuracy set for the normal velocity components has reached 10^{-7}.

The tangential velocity of the complete flow at point P on the surface of a circle can then be expressed as

$$U_\theta(P) = V[U_\theta^{\mathrm{S}}(P) + \gamma_1 \cdot U_\theta^{\mathrm{c}_1}(P) + \gamma_2 \cdot U_\theta^{\mathrm{c}_2}(P)], \tag{3.7}$$

where U_θ^{S} is the component from the streaming, $U_\theta^{\mathrm{c}_1}$ is the component due to unit circulation around the first circle, and $U_\theta^{\mathrm{c}_2}$ is the component due to unit circulation around the second circle.

3.2. *Multi-element airfoils near stall*

Instead of using the Karman–Trefftz transformations to map the two circles conformally into two airfoils as in Williams (1971), the sequence of the Joukowsky-arc model is used to create a stalled flap staggered behind the main airfoil. In fact, this model can be used for stalled flow on either element. However, the strong adverse

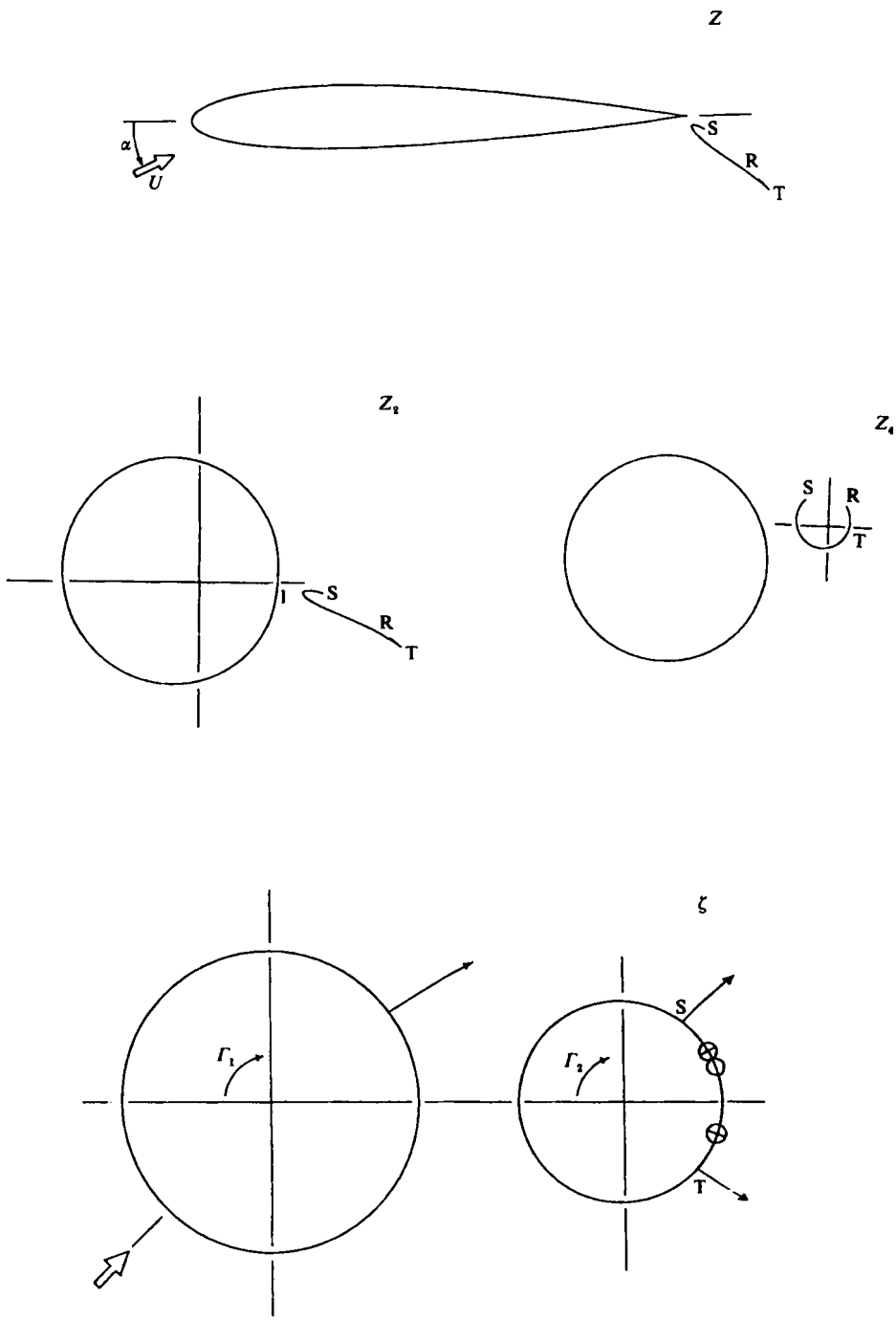

FIGURE 8. Mapping sequence for airfoil with slotted flap experiencing trailing-edge stall.

pressure gradient caused by the relatively large deflection of the flap would usually induce it to stall earlier. The following section is devoted to this situation.

As in the Joukowsky-arc model, a stalled airfoil is created in the Z_2-plane from a circle II in the ζ-plane, figure 8. Another circle I upstream of II, which would be a near-circle in the Z_2-plane, undergoes a Joukowsky transformation to become a near-

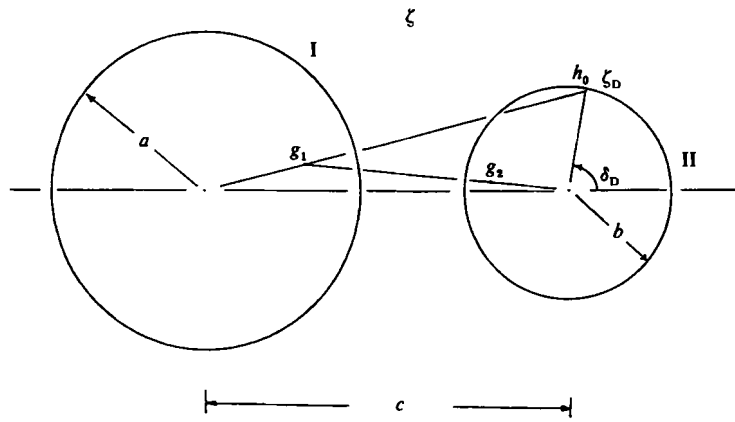

FIGURE 9. Geometry of two circles with images of a surface doublet.

Joukowsky airfoil. In the Z-plane, the two profiles, one complete and the other trailing behind with its upper surface partly omitted are both near-Joukowsky. The details of the mapping equations are

$$\zeta = Z_7 e^{i\bar{\delta}_0}, \tag{3.8}$$

$$Z_6 = C_2 Z_7 + D_2, \tag{3.9}$$

$$Z_5 = Z_6 - \cot\tilde{\alpha} - 1/(Z_6 - \cot\tilde{\alpha}), \tag{3.10}$$

$$Z_4 = A_2 Z_5 + B_2, \tag{3.11}$$

$$Z_3 = Z_4 + 1/Z_4, \tag{3.12}$$

$$Z_2 = C_1 Z_3 + D_1, \tag{3.13}$$

$$Z_1 = Z_2 + 1/Z_2, \tag{3.14}$$

$$Z = A_1 Z_1 + B_1. \tag{3.15}$$

Complex constants A_1, B_1, C_1, D_1, A_2, B_2, C_2, D_2 and angle $\bar{\delta}_0$ are for the purpose of orientation and scaling, and angle $\tilde{\alpha}$ is defined as in figure 1.

The flow model in the ζ-plane consists of the streaming and circulating components around the two circles, as discussed in §3.1. A surface source and a doublet tangent to circle II with their appropriate image systems for both circles are adopted to simulate the separated flow on the flap. The general procedure to generate the complex potentials of the doublet and its images is similar to that for the streaming flow. For a doublet of unit strength tangent to a circle at $\zeta = \zeta_D$, the complex potential is

$$h_0(\zeta) = -\frac{i e^{i\delta_D}}{\zeta - \zeta_D}, \quad \text{where} \quad \zeta_D = c + b e^{i\delta_D}. \tag{3.16}$$

Its images and their corresponding reflections are given by (as shown in figure 9)

$$g_j(\zeta) = \frac{J_j}{\zeta - L_j},$$

where for $j = 1, 3, 5, \ldots$,

$$J_j = -\frac{a^2 \bar{J}_{j-1}}{(\bar{L}_{j-1})^2}, \quad L_j = \frac{a^2}{\bar{L}_{j-1}},$$

and for $j = 2, 4, 6, \ldots$,

$$J_j = -\frac{b^2 \bar{J}_{j-1}}{(c - \bar{L}_{j-1})^2}, \quad L_j = c - \frac{b^2}{c - \bar{L}_{j-1}}$$

with $J_0 = -i e^{i\delta_D}$, $L_0 = \zeta_D$.

Therefore, the total complex potential created by the doublet and its images is

$$F^{D}(\zeta) = h_0(\zeta) + \sum_{j=1}^{\infty} g_j(\zeta). \tag{3.17}$$

In a similar manner the complex potential of a unit source located on a circle at ζ_1 and its images in two circles can be written as

$$F^{s0}(\zeta) = \frac{1}{2\pi}\ln(\zeta-\zeta_1) + \sum_{j=1}^{\infty} [f_j(\zeta)+g_j(\zeta)]. \tag{3.18}$$

The terms in the summation are

$$f_1(\zeta) = -\frac{1}{2\pi}\ln(\zeta-L_1), \quad f_2(\zeta) = \frac{1}{2\pi}\ln(\zeta-L_2),$$

$$g_1(\zeta) = -\frac{1}{2\pi}\ln(\zeta-D_1), \quad g_2(\zeta) = \frac{1}{2\pi}\ln(\zeta-D_2),$$

where

$$\zeta_1 = c+b\,e^{i\delta_S}, \quad L_1 = 0, \quad L_2 = a^2/\bar{\zeta}_1, \quad D_1 = c, \quad D_2 = c-b^2/(c-\bar{\zeta}_1).$$

In general,

$$f_j(\zeta) = -\frac{1}{2\pi}\ln(\zeta-L_j), \quad f_{j+1}(\zeta) = \frac{1}{2\pi}\ln(\zeta-L_{j+1}),$$

$$g_j(\zeta) = -\frac{1}{2\pi}\ln(\zeta-D_j), \quad g_{j+1}(\zeta) = \frac{1}{2\pi}\ln(\zeta-D_{j+1}),$$

where for $j = 3, 7, 11, \ldots,$

$$L_j = c-\frac{b^2}{c-\bar{L}_{j-2}}, \quad L_{j+1} = c-\frac{b^2}{c-\bar{L}_{j-1}}, \quad D_j = \frac{a^2}{\bar{D}_{j-2}}, \quad D_{j+1} = \frac{a^2}{\bar{D}_{j-1}}$$

and for $j = 5, 9, 13, \ldots,$

$$L_j = \frac{a^2}{\bar{L}_{j-2}}, \quad L_{j+1} = \frac{a^2}{\bar{L}_{j-1}}, \quad D_j = c-\frac{b^2}{c-\bar{D}_{j-2}}, \quad D_{j+1} = c-\frac{b^2}{c-\bar{D}_{j-1}}.$$

Therefore, the total complex potential is

$$F(\zeta) = F^{s}(\zeta) + \gamma_1 VF^{c_1}(\zeta) + \gamma_2 VF^{c_2}(\zeta) + q_S VF^{s0}(\zeta) + q_D VF^{D}(\zeta). \tag{3.19}$$

Again the series can be shown to converge absolutely. The tolerance set for truncating the series for the normal velocity components is 10^{-7} as before. The total tangential velocity at a point P on the surface of either circle is

$$U_\theta(P) = V[U_\theta^{S}(P) + \gamma_1 U_\theta^{c_1}(P) + \gamma_2 U_\theta^{c_2}(P) + q_S U_\theta^{\delta_{S0}}(P) + q_D U_\theta^{\delta_D}(P)], \tag{3.20}$$

where the first three terms within the bracket on the right-hand side are the same as those in (3.7). The fourth term is the component due to a source of strength q_S located at $\zeta_1 = c+b\,e^{i\delta_S}$. Finally, the last term is the contribution of the doublet of strength q_D at $\zeta_D = c+b\,e^{i\delta_D}$.

The boundary conditions used to determine the strengths and locations of these added singularities q_S, δ_S, q_D, δ_D and γ_1, γ_2, the circulation in each circle, are the same

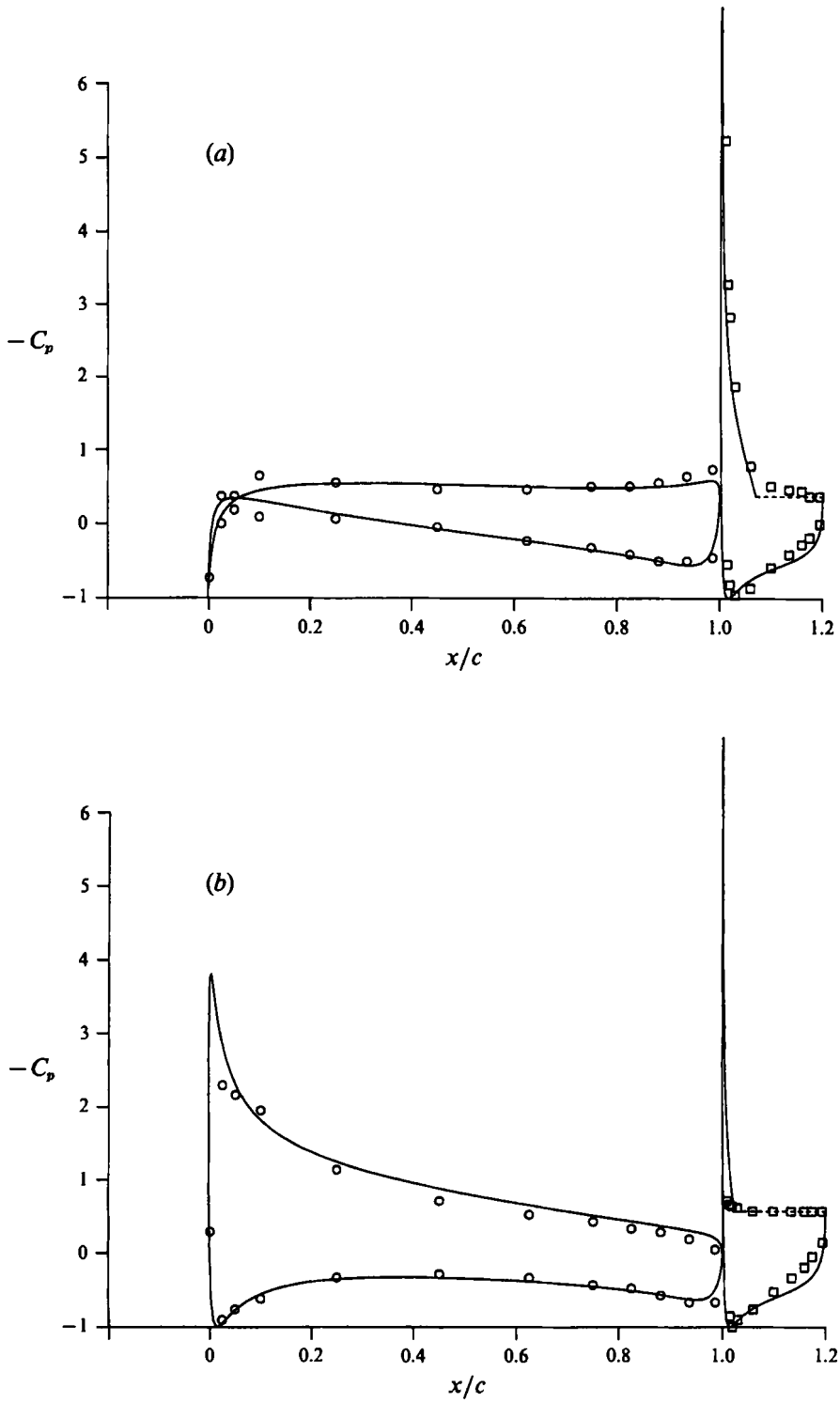

FIGURE 10. Pressure distribution for airfoil with slotted flap experiencing trailing-edge stall; 20% chord flap deflected 40°. (*a*) $\alpha = -6.9°$. ——, theory, $X_R = 0.90$, $X_S = 0.25$; C_p (wake) $= -0.545$; ○, □, experiment (Wenzinger 1938). (*b*) $\alpha = 3.16°$. ——, theory $X_R = 0.90$, $X_S = 0.05$; C_p (wake) $= -0.571$; ○, □, experiment (Wenzinger, 1938).

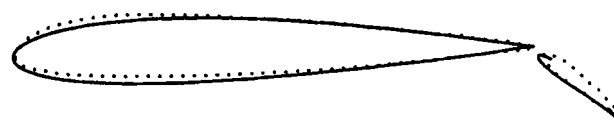

FIGURE 11. Comparison of airfoil profiles: ····, NACA23012; ——, near-Joukowsky.

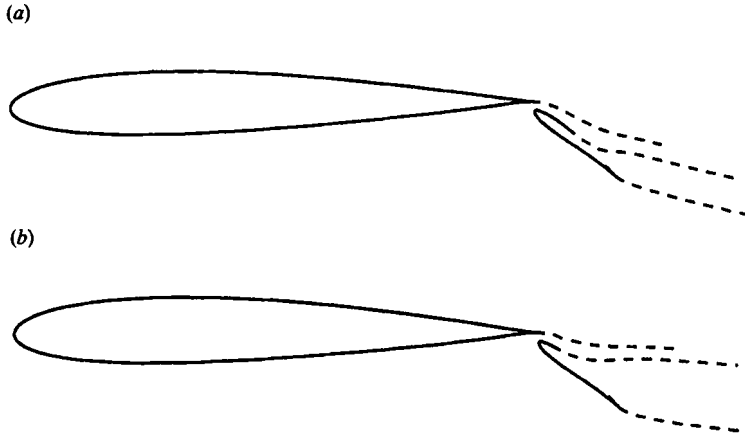

FIGURE 12. Theoretical separation streamlines; (*a*) for example of figure 10(*a*); (*b*) for example of figure 10(*b*).

as those for the Joukowsky-arc airfoil but on the flap here. In addition, tangential separation from the trailing edge of the main airfoil is enforced.

No experiments were performed on the near-Joukowsky profiles, but two representative cases using NACA 23012 profiles for main airfoil and flap were tested by Wenzinger (1938). His measured C_p distributions and the present theoretical predictions are compared with the Joukowsky profiles chosen to match the NACA profiles closely.

The two cases are for $\alpha = -6.9°$ (figure 10*a*), in which $X_S = 25\%$ chord (of the flap), C_p (wake) $= -0.545$; and $\alpha = 3.16°$ (figure 10*b*), in which $X_S = 5\%$ chord, C_p (wake) $= -0.571$. $X_R = 0.90$ was chosen for both cases. Surprisingly good agreement between theory and experiments is obtained on both elements. The discrepancy near the leading edge of the main airfoil is probably due to the inevitable differences in the airfoil shapes as shown in figure 11. Relatively high suction peaks predicted by the theory at the leading edge of the flap, $C_p = -11$ for $\alpha = -6.9°$, and $C_p = -8.6$ for $\alpha = 3.16°$, are probably caused by the 'narrow channel' bounded by the streamline from the trailing edge of the main foil and the leading edge of the flap, as shown in streamline plots, figures 12(*a*) and 12(*b*).

Recently, Williams' method has been extended to calculate flow around multi-element airfoils by Suddhoo & Hall (1985). The present model could be applied to this type of configuration, although limited to one element experiencing trailing-edge stall.

4. Discussion

The Joukowsky-arc model for single-element airfoil stall has been shown to give good agreement with experimental pressure distributions. Although the measurements have not been corrected for wind-tunnel boundary constraints, the corrections should have a negligible effect on the agreement between theory and experiment because the input pressure at separation would also be corrected. The model also gives a good

prediction of the separation streamlines. As a result, the model has been extended to two-element airfoils by adapting Williams' method. Comparisons with published data are also presented and seen to give reasonable pressure distributions.

Because the process of flow separation is boundary-layer controlled, the location and pressure at separation are required in these models, which could serve as a useful partner with a boundary-layer method in an iterative solution of the problem.

The Joukowsky-arc flow model to simulate the boundary of the wake has been altered from two sources (as in Parkinson & Jandali and P & Y) to one source plus a doublet. The doublet is preferred because it produces a separation streamline shape from the upper surface more like that of the actual shear layer.

In the flow models of this paper, the curvature or pressure gradient of the streamline is assumed finite at separation. Once again, results thus obtained show that it can be a suitable condition for flow separation taking place on bluff sections with a continuously curved contour.

The mapping sequence of the Joukowsky arc may allow models to be constructed for flow around airfoils over which separation followed by reattachment both occur tangentially. It avoids having the unrealistic stagnation points that usually occur in the above situations when modelled using potential flow. In addition, extra flow elements can be added onto the inner surface of the airfoil to give the option of specifying the required pressure along the bounding streamline, as in problems involving mixed boundary conditions. Another interesting issue that may deserve attention and further investigation is whether the criterion of finite streamline curvature or pressure gradient is applicable to flow at reattachment.

Financial support for this study was provided through a grant from the Natural Sciences and Engineering Research Council of Canada.

REFERENCES

BEARMAN, P. W., GRAHAM, J. M. R. & KALKANIS, P. 1989 Numerical simulation of separated flow due to spoiler deployment. In *Conf. Proc., Prediction and Exploitation of Separated Flow*, pp. 2.1–2.15. The Royal Aeronautical Society.

HALSEY, N. D. 1982 Comparison of the convergence characteristics of two conformal mapping methods. *AIAA J.* **20**, 724–726.

JACOB, K. 1969 Berechnung der abgelösten inkompressiblen Strömung um Tragflügelprofile und Bestimmung des maximalen Auftriebs. *Z. Flugwiss.* **17**, 221–230.

JACOB, K. 1987 Advanced method for computing flow around wings with rear separation and ground effect. *J. Aircraft*, **24**, 126–127.

MCCULLOUGH, G. B. & GAULT, D. E. 1951 Examples of three representative types of airfoil-section stall at low speed. *NACA Tech. Note* 2502.

NAKAMURA, Y. & TOMONARI, Y. 1982 The effects of surface roughness on the flow past circular cylinders at high Reynolds numbers. *J. Fluid Mech.* **123**, 363–378.

ORMSBEE, A. I. & MAUGHMER, M. D. 1986 A class of airfoils having finite trailing-edge pressure gradients. *J. Aircraft* **23**, 97–103.

PARKINSON, G. V. & JANDALI, T. 1970 A wake source model for bluff body potential flow. *J. Fluid Mech.* **40**, 577–594.

PARKINSON, G. V. & YEUNG, W. 1987 A wake source model for airfoils with separated flow. *J. Fluid Mech.* **179**, 41–57 (referred to herein as P & Y).

SCHMIEDEN, C. 1940 Flow around wings accompanied by separation of vortices. *NACA Tech. Mem.* 961.

SUDDHOO, A. & HALL, I. M. 1985 Test cases for the plane potential flow past multi-element aerofoils. *Aeronaut. J.* **89**, 403–414.

THEODORSEN, T. 1931 Theory of wing sections of arbitrary shape. *NACA Rep.* 411.

WENZINGER, C. J. 1938 Pressure distribution over an NACA 23012 airfoil with an NACA 23012 external-airfoil flap. *NACA Tech. Rep.* 614.

WILLIAMS, B. R. 1971 An exact test case for the plane potential flow about two adjacent lifting aerofoils. *R. Aeronaut. Est., Tech. Rep.* 71197.

YEUNG, W. W. H. 1990 Modelling stalled airfoils. PhD thesis, University of British Columbia.